Biosensors and Bioelectronics 66 (2015) 19–23

Contents lists available at ScienceDirect

Biosensors and Bioelectronics

journal homepage: www.elsevier.com/locate/bios

Jetting microfluidics with size-sorting capability for single-cell protease detection

Tengyang Jing [a,b], Ramesh Ramji [a], Majid Ebrahimi Warkiani [b,c], Jongyoon Han [b,d,e,*], Chwee Teck Lim [a,b,f,**], Chia-Hung Chen [a,b,g,***]

[a] Department of Biomedical Engineering, National University of Singapore, Singapore 117575, Singapore
[b] Singapore-MIT Alliance for Research and Technology (SMART) Centre, Singapore 1385602, Singapore
[c] School of Mechanical and Manufacturing Engineering, University of New South Wales, Sydney, NSW 2052, Australia
[d] Department of Electrical Engineering & Computer Science, Massachusetts Institute of Technology, Cambridge, MA 02139, United States
[e] Department of Biological Engineering, Massachusetts Institute of Technology, Cambridge, MA 02139, United States
[f] Mechanobiology Institute, National University of Singapore, Singapore 117411, Singapore
[g] Singapore Institute for Neurotechnology (SINAPSE), Singapore 117456, Singapore

ARTICLE INFO

Article history:
Received 5 August 2014
Received in revised form
22 October 2014
Accepted 1 November 2014
Available online 4 November 2014

Keywords:
Cell encapsulation
Jetting microfluidics
DLD droplet sorting
Protease biosensor
Single-cell analysis

ABSTRACT

Activated proteases such as matrix metalloproteinases (MMPs) secreted from cancer cells can degrade the extracellular matrix (ECM) and contribute to tumour formation and metastasis. Measuring MMP activity in individual cancer cells can provide important insights on cancer cell heterogeneity and disease progression. Here, we present a microfluidic platform combining a droplet jetting generator and a deterministic lateral displacement (DLD) size-sorting channel that is capable of encapsulating individual cancer cells inside picoliter droplets effectively. Droplet jetting with cell-triggered Rayleigh-Plateau instability was employed which produced large droplets capable of cell encapsulation (diameter, ~25 μm) and small empty droplets (diameter, ~14 μm), which were then size-separated using a DLD size-sorting channel to enrich the single-cell encapsulated droplets (~78%), regardless of the cell density of input sample solutions. The droplets containing encapsulated cancer cells were collected in an observation chamber to determine the kinetic profiles of MMP secretion and the inhibitory response in the presence of the drug doxycycline at the single-cell level to reveal their heterogeneous MMPs secretion activities.
© Elsevier B.V. All rights reserved.

1. Introduction

As the principal degrading enzymes of the extracellular matrix (ECM), matrix metalloproteinases (MMPs) contribute to cancer cell invasion and are potential cancer drug targets and biomarker candidates (Orlichenko and Radisky, 2008). The secretion of MMPs from cancer cells plays an important role in cancer metastasis because these enzymes break down the basal membrane and promote angiogenesis (Rundhaug, 2003). Due to their ultra-low abundance, the profile of MMPs in individual cancer cells is difficult to measure. Most MMP activity assays, such as microplate reader assays, can only determine the average reaction activity of a cell population and are therefore unable to measure variations in expression among individual cells. These assays are thus insufficiently sensitive because many critical biological signals of individual cells are masked by the major response from a pool of cells in a diverse population (Ishii et al., 2010; Lu et al., 2004).

A variety of technologies have been developed for single-cell assays. Flow cytometry is a powerful tool to determine surface biomarkers of individual cells but it cannot be used to analyse the time-lapse profile of MMP activity because only end-point measurements of stained samples are allowed (Sjostrom et al., 2014). Several microfluidic technologies have recently been developed for single-cell isolation and analysis. For example, the C1 system by Fluidigm® is based on microvalve technology to create microchamber arrays to trap single cells for genomic studies (Spurgeon et al., 2008; Zare and Kim, 2010). Similar cell compartment methods have also been developed using microwell (Jen et al., 2011; Jin et al., 2009), microtrap (Benavente-Babace et al., 2014; Di Carlo et al., 2006) and inkjet-like techniques (Yusof et al., 2011) to

* Corresponding author at: Singapore-MIT Alliance for Research and Technology (SMART) Centre, Singapore 1385602, Singapore. Fax: +1 617 258 5843.
** Corresponding author at: Mechanobiology Institute, National University of Singapore, Singapore 117411, Singapore. Fax: +65 6776 5322.
*** Corresponding author at: Department of Biomedical Engineering, National University of Singapore, Singapore 117575, Singapore. Fax: +65 6872 3069.
E-mail addresses: jyhan@mit.edu (J. Han), ctlim@nus.edu.s (C.T. Lim), biecch@nus.edu.sg (C.-H. Chen).

http://dx.doi.org/10.1016/j.bios.2014.11.001
0956-5663/© Elsevier B.V. All rights reserved.

perform a wide range of single-cell studies. However, the applications of these single-cell isolation strategies are limited by the complicated microfluidic controls and cross-cell contamination.

Droplet-based technology is attractive due to its capability for ultra-high throughput cell encapsulations (up to 10^3 droplets per second), simple fluidic control and low cross-contamination among different droplets (Brouzes et al., 2009; Konry et al., 2011). A wide range of droplet-based technologies have been developed for single-cell studies in the last decade, including applications in polymerase chain reaction (PCR) (Kumaresan et al., 2008), cell-secreted molecule (enzyme, antibody, cytokine, etc.) screening (Chokkalingam et al., 2013; Konry et al., 2011; Köster et al., 2008) and drug testing (Brouzes et al., 2009). Individual cells and reagents are encapsulated in picoliter (pL)-volume droplets, enabling a highly sensitive assay (Joensson and Andersson Svahn, 2012). Apart from these advantages, however, droplet-based single-cell assays are primarily limited by the low cell encapsulation rate, which leads to the production of large populations of empty droplets that reduce the downstream readout efficiency. In fact, cells randomly distributed in a suspension follow Poisson statistics in the encapsulation process, resulting in an ultra-low single-cell encapsulation efficiency under low cell density conditions (Köster et al., 2008).

To address the encapsulation efficiency problem, active droplet sorting systems have been developed to isolate empty droplets using gas-controlled valve (Abate and Weitz, 2008), electrical field (Baret et al., 2009) and surface acoustic wave (Franke et al., 2009). However, these systems require fluorescent staining, which would alter the cell properties and affect downstream analysis. Cell ordering prior to droplet formation has also been studied to enhance single-cell encapsulation efficiency. The single-cell encapsulation efficiency has been improved to ~80% by coupling a long straight (~5 cm) or spiral channel (~1 cm) with the droplet systems (Edd et al., 2008; Kemna et al., 2012). The cells can be ordered along the microchannel under certain flow rates to form an equally spaced cell train before encapsulation into droplets. However, these methods require extremely high cell densities (~10^7 cells/mL) to achieve effective cell encapsulation and to avoid the generation of a large number of empty droplets, limiting the application of these methods in assaying clinical samples with low cell abundance (Lagus and Edd, 2011). Moreover, hydrodynamic droplet sorting has been demonstrated to improve single-cell encapsulation rate with high input cell concentration (~10^7 cells/mL) (Chabert and Viovy, 2008). However, it is not preferable in sorting water-in-oil emulsions because the flow control of viscous oil is very difficult.

Here, we present a microfluidic platform comprising a droplet jetting generator and a deterministic lateral displacement (DLD) size-sorting channel that enables the encapsulation of individual cells into aqueous droplets in oil and facilitates the separation of cell-encapsulated droplets from empty droplets for subsequent assays. Large droplets with encapsulated cancer cells (diameter, ~25 μm) and small, empty droplets (diameter, ~14 μm) are produced based on droplet jetting with cell-triggered Rayleigh-Plateau instability. After droplet formation, size-based sorting is performed inside the DLD micro-pillar channel, where the critical dimension for separation is defined by geometric design. Continuous droplet formation and label-free sorting are achieved at a frequency of greater than 5 kHz with up to ~80% encapsulation efficiency at various cell concentrations (10^4–10^7 cells/mL). Less than 100 μL of a low-concentration cell solution is required to perform single-cell encapsulation thus allowing us to monitor the kinetic profiles of cellular MMPs, a difficult task using existing analytical methods. The heterogeneous MMP activities and varied doxycycline resistance of individual cancer cells can then be characterised. This device exhibits potential for performing functional assays of rare clinical samples, such as circulating tumour cells (CTCs).

2. Experimental methods

2.1. Microdevice design and fabrication

The microfluidic device was designed as a flow-focusing droplet generator coupled with a DLD separation channel (Fig. 1a) to overcome Poisson statistics (Supplementary-1). At the droplet-jetting region, empty droplets (diameter ~14 μm) were continuously produced. When cancer cells were encapsulated into aqueous droplets, the size of the cell-containing droplets was increased to 25 μm due to the physical size of the cancer cells (Chabert and Viovy, 2008) (Supporting Movie-1). Hence, the cell-containing droplets were 5–10 μm larger than the empty droplets (Fig. 1b). In the droplet-sorting region, only the droplets with cell encapsulations whose sizes were larger than the DLD critical dimension (20 μm) were deflected from the original direction toward the side wall (Huang et al., 2004) (Fig. 1c, Supporting Movies-2 and 3). These droplets were then collected in the observation chamber (Fig. 1d). By contrast, droplets collected from the waste outlet were empty (Fig. 1e). The integrated microdevice was fabricated by polydimethylsiloxane (PDMS) using standard soft lithography (Supplementary-2). The microdevice was mounted on an inverted microscope (Nikon Eclipse Ti) for experiments (more experimental details in Supplementary-3).

Supplementary material related to this article can be found online at 10.1016/j.bios2014.11.001.

2.2. Cell preparation and protease assay

The human non-small lung cancer cell line, PC-9, was prepared (Supplementary-4) for cell encapsulation and single-cell secreted protease assay experiments. Fluorescent cell viability assay kits

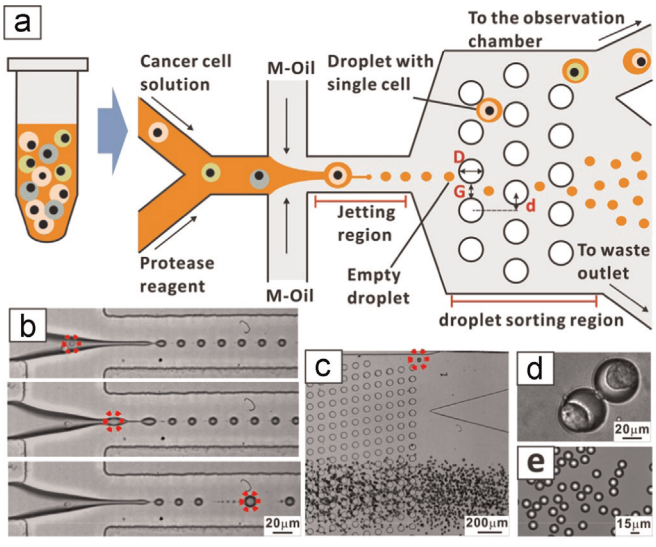

Fig. 1. (a) Schematic representation of the integrated microfluidic device comprising droplet generator and size-based sorting channel. "D", "G" and "d" refer to the size, gap, and row shift distance of micropillar array in the sorting channel, respectively. (b) Encapsulation of a cancer cell (indicated by the red-dashed circle) into a droplet with a larger size compared to other empty droplets. (c) The cell-containing droplet (indicated by the red-dashed circle) is diverted to the outlet connected to the observation chamber after passing through the sorting channel, while empty droplets proceed directly to the waste outlet. (d) Collection of two droplets with cell encapsulation in the observation chamber. (e) Removal of empty droplets from the waste outlet. (For interpretation of the references to colour in this figure legend, the reader is referred to the web version of this article.)

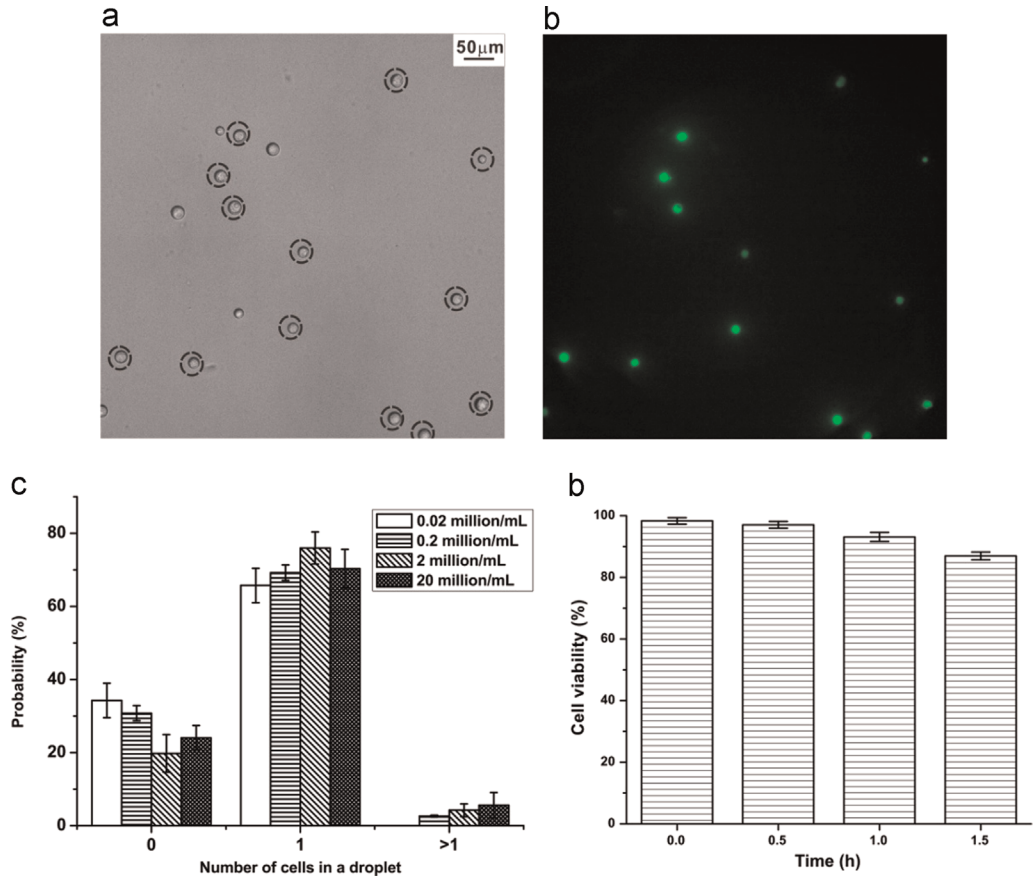

Fig. 2. (a) The bright-field and (b) the corresponding fluorescent images showing 13 stained PC-9 cells trapped in separated aqueous droplets. Scale bar is 50 μm. (c) The cell encapsulation efficiency was measured for different input cell concentrations. Due to the size-based sorting, a high encapsulation efficiency was achieved regardless of varied cell concentrations. (d) The survival rate of PC-9 cells inside droplets was measured for up to 1.5 h.

(Life Technologies) were used to evaluate cell-survival rate and facilitate cell visualisation. A fluorescent polypeptide MMP substrate (BioZyme) was applied to measure protease activity of single cells (Supplementary-5). The secreted MMPs cleaved the substrate polypeptide to induce fluorescence signals. To calibrate the droplet detection system, recombinant MMP enzyme (Enzo Life Sciences) was tested. Moreover, MMP inhibitor doxycycline (Sigma Aldrich) was applied to test its inhibitory effect on individual cancer cells at the concentration 20 μg/mL (Hanemaaijer et al., 1998; Manning et al., 2003) (Supplementary-6).

3. Results and discussion

3.1. Droplet jetting microfluidics

When an aqueous phase fluid is shorn by an immiscible oil phase from both sides, it can ultimately be broken into water-in-oil droplets via two different mechanisms: dripping or jetting. Under the dripping condition, the aqueous droplets are formed near the cross-flow junction due to the pinch effect of the oil phase. The size of droplets is usually similar to the microchannel dimension. By contrast, under jetting condition, the aqueous phase forms a thin tip that is broken into droplets away from the cross-flow junction due to Rayleigh-Plateau instability (Utada et al., 2008). Under jetting, it is possible to produce monodispersed small droplets in a relatively large channel, and the droplet size can be precisely tuned by adjusting the flow rate. Thus, the use of droplet jetting also effectively prevents channel clogging during the cell encapsulation process.

Previous studies have reported both the capillary number of the outer fluid, $C_{out}=\eta_{out}u_{out}/\gamma$, and the Weber number of the inner fluid, $W_{in}=\rho_{in}D_{orifice}u_{in}^2/\gamma$, where η_{out} is the viscosity of the outer fluid, u_{out} and u_{in} are the mean velocities of the outer and inner fluids, respectively, γ is the surface tension, ρ_{in} is the density of the inner fluid and $D_{orifice}$ is the dimension of the orifice (Utada et al., 2007). Only when the sum of C_{out} and W_{in} is larger than one order of magnitude will jetting occur. Otherwise, dripping occurs. To use jetting to achieve size distinction between cell-containing droplets and empty droplets, we chose to use viscous mineral oil (viscosity = 25.3 mPa S) as the oil phase to shear the aqueous dispersed phase. Similar experiments were conducted with fluorocarbon oils (e.g. HFE-7500 from 3M), but no jetting was observed due to the very low viscosity.

Various flow conditions of oil and aqueous solutions were tested to analyse the correlation between the flow rate and droplet size under jetting. Interestingly, we found the empty droplet size was linearly proportional to $(Q_{aqueous}/Q_{oil})^{0.5}$, where $Q_{aqueous}$ and Q_{oil} are the flow rates of the aqueous and oil solutions, respectively (Supplementary-7). When the ratio of $Q_{aqueous}$ to Q_{oil} was increased by reducing the oil flow rate or increasing the aqueous flow rate, the size of the droplets was increased. Based on the characterised relationship, the optimal flow rates to produce size distinction between empty droplets and cell-containing droplets were 0.5 μL/min for the cell solution and 20 μL/min for the oil solution. The diameter of empty droplets was 14.4 ± 0.7 μm (relative standard deviation is 4.86%) under this flow condition. The average size of PC-9 cancer cells was 13.6 μm, which expanded the cell-containing droplet to 25 μm in diameter. The 10 μm size difference was produced for the subsequent size-based sorting.

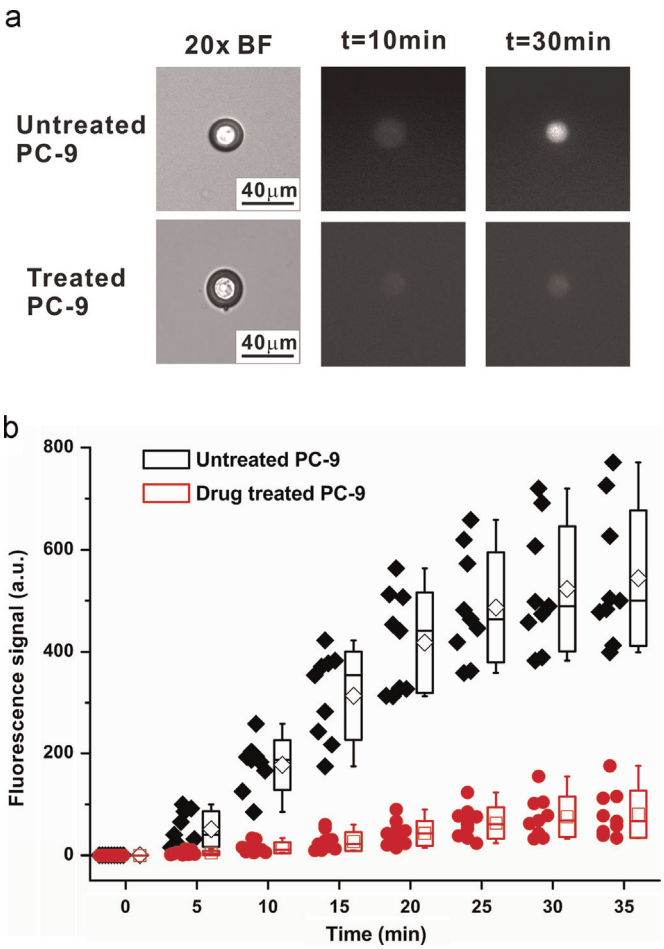

Fig. 3. (a) Images of untreated and doxycycline-treated single PC-9 cells inside droplets displaying different MMP activities. Compared to the signals from treated cells, stronger fluorescent intensity increases yielded from untreated cancer cell were observed. (b) Fluorescent signals from individual untreated and doxycycline-treated cells results, demonstrating the heterogeneity in MMP activities among cancer cells and the MMP inhibitory effect of doxycycline. Scattered points: data points for single cells; box plots: mean, medium, standard deviation, minimum and maximum values.

3.2. Size-based droplet sorting

A deterministic lateral displacement (DLD) micropillar array was connected to the droplet jetting generator to sort the larger droplets containing encapsulated cells from the smaller empty droplets for effective downstream single-cell measurement. Based on the aforementioned droplet size difference, the critical dimension of separation D_C was set to 20 μm (Supplementary-8). The small empty droplets whose diameters were below the critical dimension of the DLD separation followed their original flowing direction inside the micropillar array, heading to the waste outlet. The droplets containing an encapsulated cell, whose diameters were above the critical dimension, were deflected from their original direction toward the side wall and trapped in the observation chamber.

Freshly harvested PC-9 cancer cells were first labelled using green fluorescent calcein-AM live stain and then mixed with density gradient medium to prevent cell sedimentation in the syringe during the experiments. Based on both bright-field and fluorescent images observed under a fluorescence microscope (Fig. 2a and b), the presence of individual cells in the droplets could be recorded to calculate the cell encapsulation rate. Four different cell concentrations (2×10^4, 2×10^5, 2×10^6, and 2×10^7 cells/mL) were tested. High single-cell encapsulation efficiencies were obtained regardless of the cell concentrations in the sample solutions, yielding better performance than that predicted by the Poisson model. For instance, the single-cell rate of the random encapsulation process was as low as 0.02% for the cell solution with a concentration of 2×10^4/mL, whereas the developed device could achieve a single-cell rate of ~78%. The single-cell encapsulation efficiency represented by the middle four columns of Fig. 2c demonstrates that the efficiency reached its minimum at 60% when the input cell concentration was 2×10^4/mL and its maximum at 78% when the input cell concentration was 2×10^6 /mL. A slight decrease in the single-cell encapsulation rate was observed at the both lowest and highest cell concentrations, which might be due to the random formation of some large empty droplets resulting from flow fluctuations and the formation of a small fraction of cell clusters during the cell sample preparation steps that eventually generated multi-cell encapsulation in one droplet.

Cell viability tests were performed after sorting. The viability of PC-9 cells was evaluated every half an hour by counting the number of viable and dead cells by fluorescence microscopy. The viability ratios at different time points are reported in Fig. 2d. It was approximately 90% after 1 h of cell encapsulation. Therefore, the duration of the subsequent single-cell MMP assay experiments was restricted to less than 1 h.

3.3. Single cancer cell MMP assay

Before conducting the single cancer cell MMP assays, recombinant MMP-9 enzyme at various concentrations was first tested with the polypeptide MMP substrate to correlate the MMP concentrations with the fluorescence signal read-out (Supplementary-9). After characterizing pure MMP recombinants, MMPs secreted from individual PC-9 cells were characterised by encapsulating the MMP substrate with cell solution into droplets. The secreted MMPs cleaved the substrate polypeptide to yield fluorescence that sigmoidally increased in intensity with reaction time, as shown in Fig. 3a. The fluorescence intensity increased at a slow rate in the beginning of the MMP assays and grew fast after some time, because the amount of MMPs accumulated gradually with the slow secretion process. The fluorescent signals eventually saturated at ~35 min due to the MMP substrate depletion. Based on the measured fluorescent intensities, cancer cell heterogeneity in the MMP activities could clearly be observed, with an increase in intensity from 400 to 800 a.u. over 35 min. Based on the results obtained from pure MMP test, after fluorescence signal to enzyme concentration conversion (Supplementary-10), a range of ~1.5–3 nM active MMPs was secreted from individual live PC-9 cancer cells in 35 min. Notably, to ensure the accuracy of the fluorescent-based assay, the time gap between droplet generation and the final assay was strictly controlled. The time period for a droplet to travel from the reagent mixing area to the observation chip was ~30 s, and the time required to fill the observation chip was ~2 min; these times are both much shorter than the MMP saturation time period (~30 min). Therefore, the readout time points for each cell-containing droplet were approximately the same, and the slopes of the fluorescence increases could be used to represent the MMP activities.

The inhibition of the MMP activities of individual PC-9 cancer cells in response to the treatment with doxycycline was then analysed. The presented microfluidic device enabled continuous monitoring of the effects of doxycycline on individual cancer cells for up to 1 h. Different levels of suppression of MMP activities at the same dose of doxycycline were recorded, revealing heterogeneity in the resistance of PC-9 cancer cells against doxycycline. In general, the MMP activities were greatly suppressed by doxycycline, as evidenced by the reduction in the increase in

fluorescence exhibited by the droplet to 100 a.u. over 35 min (Fig. 3b). The inhibition observed in the single-cell droplets system is larger than that observed in conventional plate reader assays in which a cancer cell population is analysed (Supplementary-11). After signal conversion, the concentration of active MMPs secreted by individual doxycycline-treated PC-9 cells was reduced to a range of 0.2–0.5 nM. However, a few individual cancer cells retained some MMP activities under doxycycline treatment, which might suggest that a small group of cancer cells could quickly develop doxycycline resistance, even in the clonally cultured cancer cell line.

4. Conclusion

An integrated microfluidic device combining a droplet jetting component and a DLD sorting channel was developed for effective single-cell encapsulation, enabling assays of cell-secreted MMPs using minute quantities of reagents. The single-cell encapsulation rate was increased to 78%, at an input cell concentration of 10^6 cells/mL, in contrast to the 1.6% rate predicted by the Poisson statistics. Single cancer cell protease assays were performed by measuring MMP secretion from the individual PC-9 cancer cells inside droplets. Heterogeneous MMP activities and various levels of drug resistance were observed at the single-cell level. The concentration of MMPs secreted from individual PC-9 cells was in the range of 1.5–3 nM. After doxycycline treatment, the concentration of MMPs secreted by individual cells was suppressed to within 0.2–0.5 nM. We believe that our hybrid microfluidic system is ideal for the analysis of enzymatic activity at the single-cell level in samples with low cell concentrations (e.g. 10^4 cells/mL), because our method eliminates the need for immune-staining and active sorting. With further development, our platform can be used for direct physiological analysis of unprocessed clinical samples with low cancer cell concentrations for rapid diagnostics and customised cancer therapeutics.

Acknowledgement

We thank the financial support from NUS start-up Grant (R397-000-137-133), SMART innovation Grant (R397-000-146-592), Tier-1 Grant (R-397-000-153-112), and SMART BioSym Inter-Disciplinary Research programme. The PC-9 cancer cell lines were accepted as a kind gift from Dr. Daniel Tan of the National Cancer Centre, Singapore. All the silicon wafer fabrication was kindly done at the Nano and Microfabrication Core of the Mechanobiology Institute (MBI) at the National University of Singapore.

Appendix A. Supplementary Information

Supplementary data associated with this article can be found in the online version at 10.1016/j.bios2014.11.001.

Reference

Abate, A., Weitz, D., 2008. Appl. Phys. Lett. 92 (24), 243509.
Baret, J.-C., Miller, O.J., Taly, V., Ryckelynck, M., El-Harrak, A., Frenz, L., Rick, C., Samuels, M.L., Hutchison, J.B., Agresti, J.J., 2009. Lab Chip 9 (13), 1850–1858.
Benavente-Babace, A., Gallego-Pérez, D., Hansford, D.J., Arana, S., Pérez-Lorenzo, E., Mujika, M., 2014. Biosens. Bioelectron. 61 (0), 298–305.
Brouzes, E., Medkova, M., Savenelli, N., Marran, D., Twardowski, M., Hutchison, J.B., Rothberg, J.M., Link, D.R., Perrimon, N., Samuels, M.L., 2009. Proc. Natl. Acad. Sci. 106 (34), 14195–14200.
Chabert, M., Viovy, J.-L., 2008. Proc. Natl. Acad. Sci. 105 (9), 3191–3196.
Chokkalingam, V., Tel, J., Wimmers, F., Liu, X., Semenov, S., Thiele, J., Figdor, C.G., Huck, W.T., 2013. Lab Chip 13 (24), 4740–4744.
Di Carlo, D., Aghdam, N., Lee, L.P., 2006. Anal. Chem. 78 (14), 4925–4930.
Edd, J.F., Di Carlo, D., Humphry, K.J., Köster, S., Irimia, D., Weitz, D.A., Toner, M., 2008. Lab Chip 8 (8), 1262–1264.
Franke, T., Abate, A.R., Weitz, D.A., Wixforth, A., 2009. Lab Chip 9 (18), 2625–2627.
Hanemaaijer, R., Visser, H., Koolwijk, P., Sorsa, T., Salo, T., Golub, L.M., Van Hinsbergh, V., 1998. Adv. Dent. Res. 12 (1), 114–118.
Huang, L.R., Cox, E.C., Austin, R.H., Sturm, J.C., 2004. Science 304 (5673), 987–990.
Ishii, S., Tago, K., Senoo, K., 2010. Appl. Microbiol. Biotechnol. 86 (5), 1281–1292.
Jen, C.-P., Hsiao, J.-H., Maslov, N.A., 2011. Sensors 12 (1), 347–358.
Jin, A., Ozawa, T., Tajiri, K., Obata, T., Kondo, S., Kinoshita, K., Kadowaki, S., Takahashi, K., Sugiyama, T., Kishi, H., 2009. Nat. Med. 15 (9), 1088–1092.
Joensson, H.N., Andersson Svahn, H., 2012. Angew. Chem. Int. Ed. 51 (49), 12176–12192.
Kemna, E.W., Schoeman, R.M., Wolbers, F., Vermes, I., Weitz, D.A., van den Berg, A., 2012. Lab Chip 12 (16), 2881–2887.
Konry, T., Dominguez-Villar, M., Baecher-Allan, C., Hafler, D.A., Yarmush, M.L., 2011. Biosens. Bioelectron. 26 (5), 2707–2710.
Köster, S., Angile, F.E., Duan, H., Agresti, J.J., Wintner, A., Schmitz, C., Rowat, A.C., Merten, C.A., Pisignano, D., Griffiths, A.D., 2008. Lab Chip 8 (7), 1110–1115.
Kumaresan, P., Yang, C.J., Cronier, S.A., Blazej, R.G., Mathies, R.A., 2008. Anal. Chem. 80 (10), 3522–3529.
Lagus, T., Edd, J., 2011. J. Vis. Exp. 64, e4096.
Lu, X., Huang, W.H., Wang, Z.L., Cheng, H.K., 2004. Anal. Chim. Acta 510 (2), 127–138.
Manning, M.W., Cassis, L.A., Daugherty, A., 2003. Arterioscler. Thromb. Vasc. Biol. 23 (3), 483–488.
Orlichenko, L., Radisky, D., 2008. Clin. Exp. Metastasis 25 (6), 593–600.
Rundhaug, J.E., 2003. Clin. Cancer Res. 9 (2), 551–554.
Sjostrom, S.L., Bai, Y., Huang, M., Liu, Z., Nielsen, J., Joensson, H.N., Andersson Svahn, H., 2014. Lab Chip 14 (4), 806–813.
Spurgeon, S.L., Jones, R.C., Ramakrishnan, R., 2008. PloS One 3 (2), e1662.
Utada, A.S., Fernandez-Nieves, A., Gordillo, J.M., Weitz, D.A., 2008. Phys. Rev. Lett. 100 (1), 014502.
Utada, A.S., Fernandez-Nieves, A., Stone, H.A., Weitz, D.A., 2007. Phys. Rev. Lett. 99 (9), 094502.
Yusof, A., Keegan, H., Spillane, C.D., Sheils, O.M., Martin, C.M., O'Leary, J.J., Zengerle, R., Koltay, P., 2011. Lab Chip 11 (14), 2447–2454.
Zare, R.N., Kim, S., 2010. Annu. Rev. Biomed. Eng. 12, 187–201.